

$FLAC^{3D}$ mesh and zone quality

B. Abbasi

Southern Illinois University, Carbondale, IL, USA

D. Russell & R. Taghavi

Itasca Consulting Group, Inc., Minneapolis, MN, USA

ABSTRACT: Mesh quality is crucial for the stability, accuracy, and fast convergence of numerical simulations. However, given the geometrical complexity of some models and the tools available for mesh creation, it is often necessary to accept meshes that deviate significantly from the known ideal shape. Since mesh generation can be a very time-consuming process, it is also necessary to be able to judge if a given mesh will perform well enough for a given model or if more effort needs to be made to improve its quality. There are many well-understood rules of thumb for judging mesh quality in Finite-Element applications, but these rules do not apply to the Lagrangian finite-volume with mixed-discretization approach used by $FLAC^{3D}$ zones. The goal of this study is to determine simple metrics that allow a user to judge how deformed the initial shape of $FLAC^{3D}$ zones can be before they begin to significantly affect the quality of the solution.

1 INTRODUCTION

High-quality meshes are essential for accuracy in a numerical model. With the help of partial differential equations (PDEs), Knupp (2007) showed how the quality of the mesh can affect the accuracy and efficiency of numerical simulations. There are many studies on the subject of determining good mesh quality metrics (Stimpson 2007, Pebay 2004, Knupp 2003, 2007, Kwok & Chen 2000 and Robinson 1987). They all agree that element shape is an important parameter in final result accuracy. Even a few poorly-shaped elements can cause significant error. It is therefore important to be able to identify and correct these problems at the start of model creation.

Aspect ratio, orthogonality (interior angle), face planarity, skew and taper are the most common measures of the quality of structured elements. Over the past decade, aspect ratio and orthogonality have become more important and are widely used quality measures for 2-dimensional and 3-dimensional elements.

There are three main types of mesh quality improvement techniques: adaptivity (Chalasani et al. 2002, Klein 1999), smoothing (Freitag & Plassmann 2000, Amenta & Eppstein 1997), and edge or face swapping (Freitag & Ollivier 1997, Joe 1995). In mesh smoothing techniques the coordinates of nodes (grid point) are altered without changing the connectivity of the vertices. Because of this advantage the mesh smoothing technique was employed in this paper, specifically by generating a mesh with a given topology and then moving the grid-points to match the desired level of deformation.

$FLAC^{3D}$ can measure three functions (orthogonality, aspect ratio and face planarity) which allow the users to view mesh metric information and thereby evaluate the mesh quality. In the presented paper orthogonality and aspect ratio were tested. The purpose of this paper is to estimate the relative error caused by a deformed mesh in comparison to the ideal mesh pattern. For this purpose, three typical problems with well-defined analytical solutions were selected.

The methodology and analytical solutions of these problems are discussed in the following section.

2 PROBLEM STATEMENT AND ANALYTICAL SOLUTION

2.1 Two-dimensional mesh assessment

For testing two-dimensional mesh element quality, two traditional problems with well documented closed-form solution were selected. The detailed problem statements and analytical solutions are discussed below. All of these problems were chosen from the *FLAC^{3D}* manual (Itasca 2012).

2.1.1 Cylindrical hole in an infinite Mohr-Coulomb material

In this problem, stresses are determined numerically and analytically for the case of a cylindrical hole in an infinite elasto-plastic material subjected to in-situ stresses. The material is assumed to be linearly elastic and perfectly plastic, with a failure surface defined by the Mohr-Coulomb criterion. Associated flow rules (dilatancy = friction angle) are used in the simulation. The results of the simulation are compared with an analytic solution. This problem tests the Mohr-Coulomb plasticity model with plane-strain conditions imposed in *FLAC^{3D}*. The Mohr-Coulomb material is assigned the following properties (Table 1):

Table 1. Material properties.

Shear Modulus	Bulk Modulus	Cohesion	Friction Angle	Dilation Angle
2.8 GPa	3.9 GPa	3.45 MPa	30°	30°

Stresses of 30 MPa were applied as initial conditions and to the far field, and the pressure inside the hole was neglected. Remember that in *FLAC^{3D}* compressive stresses are negative. The radius (a) of the hole is small compared to the length of the cylinder, so plane-strain conditions are applicable.

2.1.1.1 Closed-form solution

The analytical solution of this problem was developed by Salençon (1969). The detailed solution can be found in the Verification Problems volume of the *FLAC^{3D}* manual (Itasca 2012).

2.1.2 Rough strip footing on a cohesive frictionless material

The classic “Prandtl’s Wedge” problem was selected for the second test of two-dimensional mesh element quality. Stresses were determined both numerically and analytically. Prediction of the collapse loads under steady plastic-flow conditions can be difficult for a numerical model to simulate accurately (Sloan and Randolph, 1982). As a two-dimensional example of a steady-flow problem, we consider the determination of the bearing capacity of a strip footing on a cohesive *frictionless* material (Tresca model). The value of the bearing capacity is obtained when steady plastic flow has developed underneath the footing, providing a measure of the ability of the code to model this condition. The strip footing is located on an elasto-plastic material with the following properties (Table 2):

Table 2. Material properties.

Shear Modulus	Bulk Modulus	Cohesion	Friction Angle	Dilation Angle
0.1 GPa	0.2 GPa	0.1 MPa	0°	0°

2.1.2.1 Closed-form solution

The bearing capacity obtained as part of the solution to the “Prandtl’s Wedge” problem is given by Terzaghi & Peck (1967) as:

$$q = (2 + \pi)c \quad (1)$$

in which q is the average footing pressure at failure, and c is the cohesion of the material. The corresponding failure mechanism is illustrated in Figure 1.

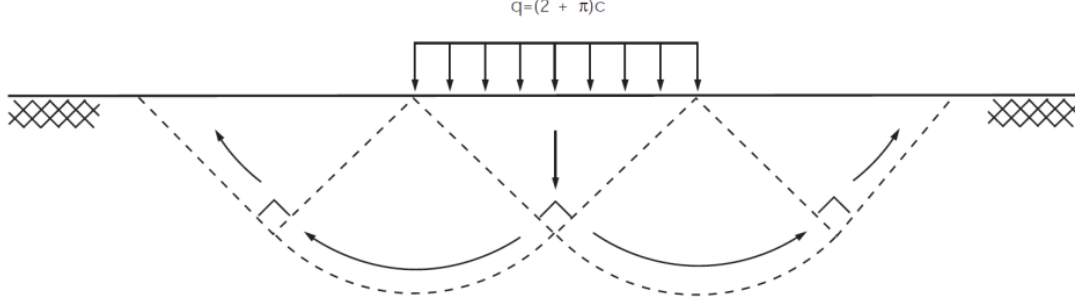


Figure 1. Prandtl mechanism for a strip footing.

2.2 Three-dimensional assessment:

For testing three-dimensional mesh elements quality, a smooth square footing problem was selected. The detailed problem statement and analytical solution are discussed below:

2.2.1 Smooth square footing on a cohesive frictionless material

This problem is concerned with the numerical and analytical determination of the bearing capacity of a smooth rectangular footing on a cohesive frictionless material (Tresca model). The footing of width ($2a$) and length ($2b$) is located on an elasto-plastic Tresca material.

2.2.1.1 Closed-form solution

The problem is truly three-dimensional. Although no exact solution is available, upper and lower bounds for the bearing capacity (q) defined as the average footing pressure at failure, have been derived using limit analysis (see, for example, Chen 1975). The upper bound, q^u , is obtained using the failure mechanism of Shield & Drucker (1953), in the form of

$$q^u = c \left(5.24 + 0.47 \frac{a}{b} \right) \frac{a}{b} \geq 0.53$$

$$q^u = c \left(5.14 + 0.66 \frac{a}{b} \right) \frac{a}{b} < 0.53 \quad (2)$$

in which c is the cohesion of the material. The lower bound, q^l , which corresponds to the bearing capacity of a strip footing, has the value

$$q^l = c(2 + \pi) \quad (3)$$

3 ELEMENTS QUALITY CALCULATION:

3.1 Aspect ratio

We define Aspect Ratio as the ratio of the longest edge of an element to either its shortest edge or the shortest distance from a corner node to the opposing edge. This paper considers two loading directions, called pattern one and two. As seen in Figure 2, pattern one orients the longer edges vertically and pattern two orients them horizontally.

For sensitivity analysis, 15 different aspect ratios between 1 ($AS = 1$) to 20 ($AS = 20$), were selected. To capture the effect of the number of zones and aspect ratios on the final results, each problem was repeated with 40 different mesh discretization patterns. A total of 2400 models were run for aspect ratio sensitivity analysis.

3.2 Orthogonality

For each element, orthogonality is defined as the ratio of the smallest angle to the largest angle. The quantities compare the hexahedron to a perfect cube, which gives 1.0 for a cube, and approaches zero as pairs of edges approach being coplanar. Figure 3 shows the calculation of orthogonality.

For sensitivity analysis, nine different orthogonality ratios, between one ($OR = 1$, representing a perfect cube) to 0.058 ($OR = 0.058$, represent $\alpha = 10$ and $\beta = 170$), were selected. To capture the effects of the number of zones and orthogonality ratios on the final results, each problem was repeated with forty different mesh discretization patterns. A total of 1080 models were simulated for orthogonality sensitivity analysis.

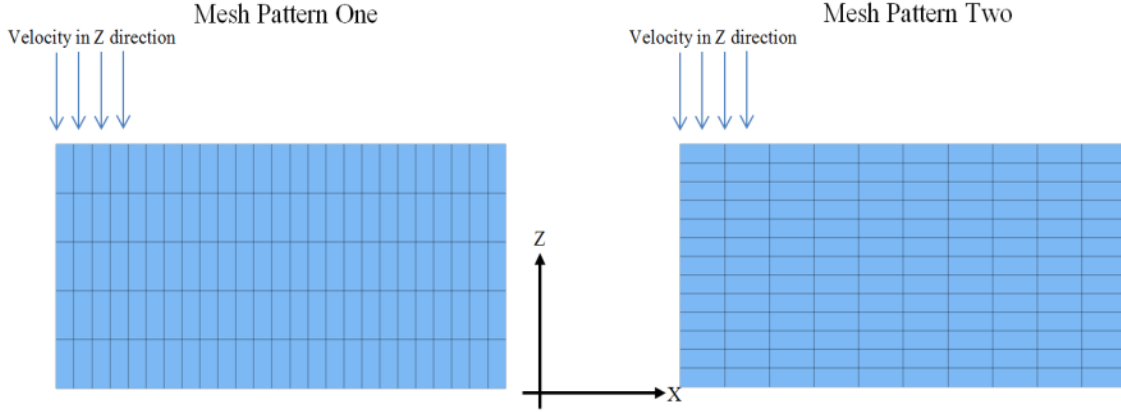


Figure 2. Aspect ratio and loading directions (pattern one and two) with respect to the orientation of the longest edge of an element to its shortest edge.

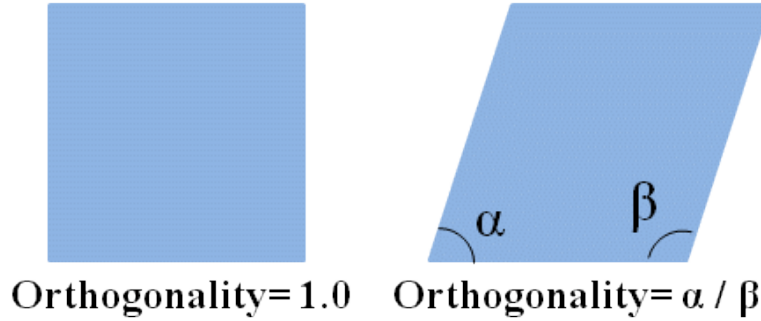


Figure 3. Definition of the orthogonality.

3.3 Element shape

Four typical element shapes were considered: brick, wedge, pyramid and tetrahedron. In *FLAC^{3D}* uses a mixed discretization technique to overcome overly stiff elements and give elements more volumetric flexibility without introducing unconstrained degrees-of-freedom. In mixed discretization a zone (element) is made of an assembly of two overlapping groups of n_t tetrahedrons, as illustrated in Figure 4 (for the case $n_t = 5$) (Itasca 2012). Bricks, wedge, pyramids, and tetrahedra are assemblies of ten, six, four, and two tetrahedra, respectively. Since this drastically changes the actual computational cost for the same number of elements of different types, the number of internal tetrahedra per-volume of interest (NTV) was calculated and used for comparison.

To capture effects of the number of zones and element shapes on the final results, each problem was repeated with forty different mesh discretization patterns. A total of 480 models were run for element shapes sensitivity analysis.

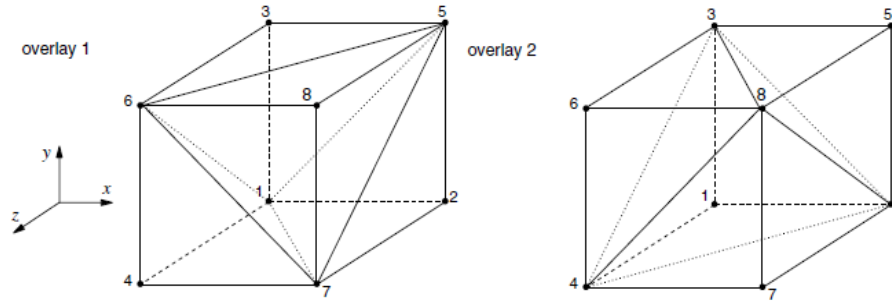


Figure 4. Brick element zone with 2 overlays of 5 tetrahedra in each overlay (Itasca 2012).

4 MODEL DEVELOPMENT

Three models were simulated for mesh sensitivity analysis. Relative error and absolute error are used to compare the results of the three models. Assuming cubic mesh elements as an ideal mesh pattern (with zero error), relative error (RE) is defined as an additional error due to change of element shape and absolute error is the discrepancy between the close form solution and numerical results. Table 3 summarizes each model.

Table 3. Matrix of models analyzed.

Model name	Model	Method	Description
Cylindrical Hole	Model 1	-Two-Dimensional -Analytical	-Mohr-Coulomb Material -Aspect ratio, orthogonality and element shape test
Rough Strip Footing	Model 2	-Two-Dimensional -Analytical	-Cohesive Frictionless Material -Mohr-Coulomb Material -Aspect ratio, orthogonality and element shape test
Smooth Square Footing	Model 3	-Three-Dimensional -Analytical	-Cohesive Frictionless Material -Mohr-Coulomb Material -Aspect ratio, orthogonality and element shape test

4.1 Model 1

This model is defined by the domain sketched in Figure 5a. The symmetric nature of the problem allows us to model one quarter of the geometry. The far x- and z-boundaries are situated at a distance of five hole-diameters from the axis of the hole. The thickness of the domain is selected as one-tenth of the hole diameter. The boundary conditions applied to this domain are sketched in Figure 5b, and they include a stress boundary of 30 MPa on the far field surfaces. The region of interest is calculated as shown in Figure 5b. The model starts with a uniform stress of 30 MPa throughout the domain and then the hole is removed.

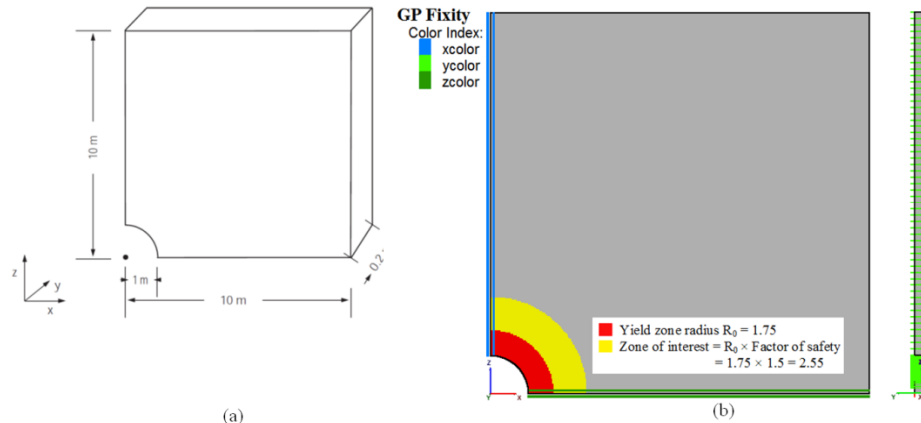


Figure 5. a) Domain for model 1 simulation – quarter symmetry, b) boundary conditions for model 1 and illustration of zone of interest – quarter symmetry.

4.2 Model 2

For this problem, half-symmetry and plane-strain conditions are assumed in the numerical simulation. The domain used for the analysis is sketched in Figure 6a. The area representing the strip footing has a half-width (a), the far x -boundary is at a distance of 20 m from the y -axis of symmetry, and the far z -boundary is located 10 m below the footing. The thickness of the domain is selected as 1 m. The boundary conditions applied to this domain are shown in Figure 6b. The displacement of the rough footing is restricted in the y -direction, and a velocity with the magnitude of 0.5×10^{-5} m/step is applied to the model in the negative z -direction to simulate the footing load. Prandtl's plastic equilibrium theory was used for calculating the region of interest, and for the sake of simplicity, the plastic zone is assumed to be rectangular (Fig. 6b).

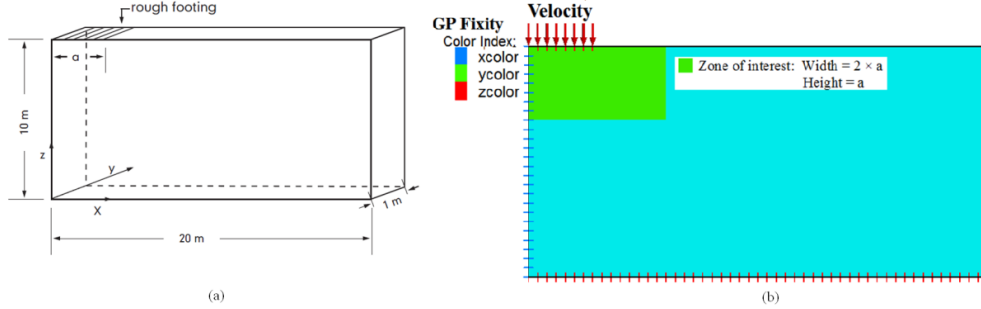


Figure 6. a) Domain for model 2 simulation – half symmetry, b) boundary conditions for model 2 and illustration of zone of interest– half symmetry.

4.3 Model 3

For this problem, the footing is square and represented by an area with half-width (a) and ($b = a$). The symmetric nature of the problem allows us to model one quarter of the geometry, and a parallelepiped domain of 15 m \times 15 m \times 10 m (as depicted in Fig. 7a) is used in the numerical simulation. The boundary conditions applied to this domain are sketched in Figure 7b. The displacements of the far x -, y - and z -boundaries are restricted in all directions and the displacements of the symmetry boundaries corresponding to the planes at $x = 0$ and $y = 0$ are restricted in the x - and y -directions, respectively. Displacements are free in the x - and y -directions and a velocity with the magnitude of 2.5×10^{-5} m/step is applied in the positive z -direction to grid points within a 3 m \times 3 m area to simulate loading of the footing. For the applied velocity loading, the bearing area is assumed to extend to half the distance between the last applied grid point and the next grid point. In this model, then, $a = 3.5$ m and $b = 3.5$ m (Fig. 7b).

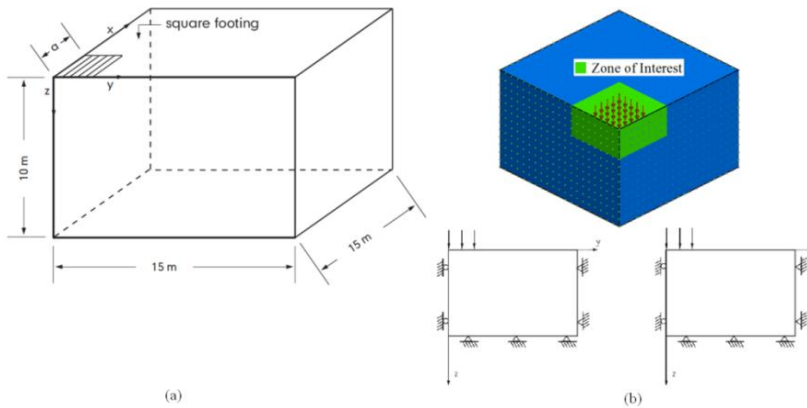


Figure 7. a) Domain for model 3 simulation – quarter symmetry, b) boundary conditions for model 3 and illustration of zone of interest– quarter symmetry.

5 RESULTS AND DISCUSSION

5.1 Cylindrical hole in an infinite Mohr-Coulomb material (model 1)

The effects of aspect ratio, orthogonality and element shape in a typical cylindrical geometry were analyzed. Fifteen aspect ratios ($AR = 1$ to 20), nine orthogonality ratios ($OR = 1$ to 0.058) and four element shapes (brick, wedge, pyramid and tetrahedron) with different mesh densities ($NTV = 5$ to 123) were selected. Figure 8 shows a typical comparison between $FLAC^{3D}$ results and the analytical solution along a radial line with $AR = 1$ and $NTV = 50$. Normalized stresses ($-\sigma_r/P_0$ and $-\sigma_\theta/P_0$) are plotted versus the normalized radius, r/a . The average relative error on the stresses and displacements is less than 1.5%.

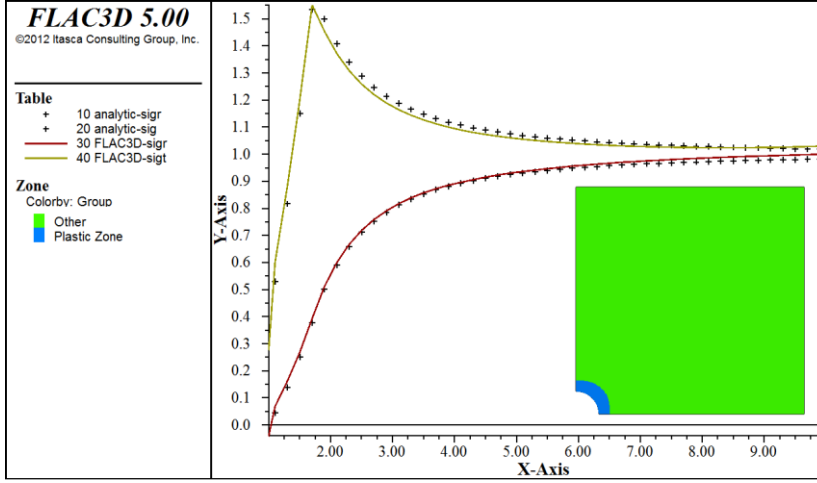


Figure 8. Stress and plastic zone comparison between analytical and $FLAC^{3D}$ solution.

Figure 9a shows the relative error of the radial stress versus different values of aspect ratios for NTV of 10, 20, 30 and 50. For comparison, it is assumed that a mesh element with $AR = 1$ (equal size element) is an ideal mesh with relative error of zero. The results show that relative error remains less than 5% when AR increases from 1.0 to 7.5. Increasing NTV (mesh density) does not improve the problem resolution significantly. In the case of a coarse mesh ($NTV = 10$) relative errors are between 5% and 10% for $AR = 6.0$ to 15.0 , but relative errors increase significantly for AR values more than 12.5. For relatively fine meshes ($NTV = 20$ and 30) relative errors are less than 10% for a range of AR from 1.0 to 15.0 , but this value increases significantly when AR exceeds 15.0. For an extremely fine mesh ($NTV = 50$), relative errors remain below 10% even for $AR = 20.0$.

Figure 9b shows the relative error of the radial stress versus different orthogonality ratios (OR) for NTV values of 10, 20, 30 and 50. For comparison, it is assumed that a mesh element with $OR = 1.0$ (corresponding to right angle) is an ideal mesh with relative error of zero. The results show that relative error remains below 5% as OR varies from 1.0 to 0.38 (corresponding to an acute angle of 30 degrees). Increasing the NTV (mesh density) does not improve the accuracy of the results significantly. However, for OR values less than 0.44 (or acute angle of less than 40 degree) the relative error increases significantly.

Figure 9c shows the absolute error (the numerical analysis results are compared with the close form solution results) in the radial stress versus different mesh element shapes for NTV values of 10, 20, 30, 50 and 60. The results show that the brick element shape yields the lowest absolute error and a tetrahedral element produces the largest error. Between wedge and pyramid mesh shapes, wedge element shows slightly better performance. By choosing an appropriate mesh density (in this problem $NTV \geq 30$) the absolute error is less than 5% for the three mesh shapes of brick, wedge and pyramid. However, tetrahedral elements perform poorly even with an extremely fine mesh size (error = 15% for $NTV = 60$).

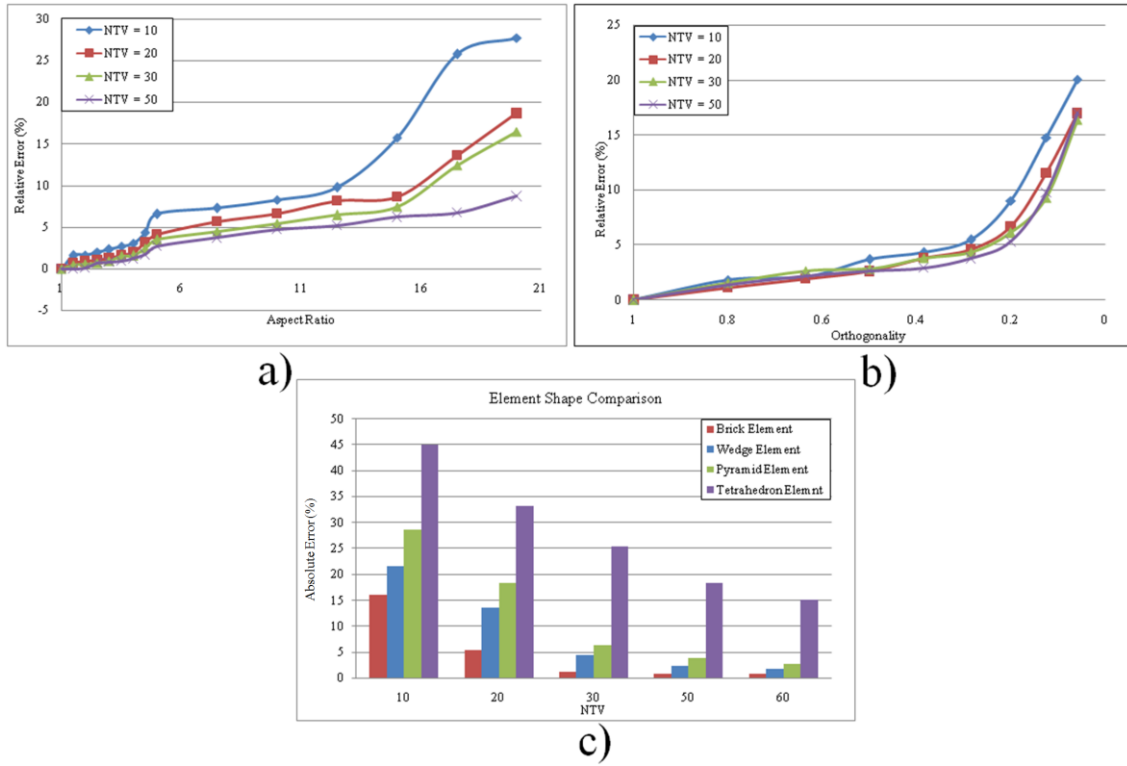


Figure 9. a) Aspect ratio sensitivity analysis for cylindrical hole in an infinite Mohr-Coulomb material, b) Orthogonality sensitivity analysis for cylindrical hole in an infinite Mohr-Coulomb material, c) Element shape sensitivity analysis for cylindrical hole in an infinite Mohr-Coulomb material.

5.2 Rough strip footing on a cohesive frictionless material (model 2)

The effects of aspect ratio, orthogonality and element shape in a typical strip foundation problem were analyzed. Fifteen aspect ratios ($AR = 1$ to 20), nine orthogonality ratios ($OR = 1$ to 0.058) and four element shapes (brick, wedge, pyramid, and tetrahedron) with different mesh densities ($NTV = 5$ to 93) were selected. The load-displacement curve corresponding to the numerical simulation is presented in Figure 10, where p-load is the normalized average footing pressure (p/c) and c-disp is the magnitude of the normalized vertical displacement (u_z/a) at the center of the footing. The numerical value of the bearing capacity (q) is 515.0 kPa, and the relative error is 0.2% when compared to the analytical value of 514.2 kPa.

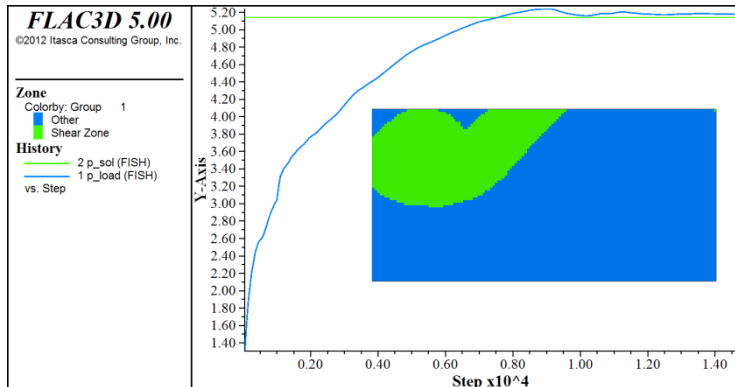


Figure 10. Stress and plastic zone comparison between an analytical and $FLAC^{3D}$ solution.

The effect of the angle of load direction compared to the direction of the longest edge of an element or its shortest edge is unknown (pattern one and two section 3.1). To test this, the vertical load in the pattern one and two is applied perpendicularly to the shortest and the longest edge of elements, respectively. Figure 11a, b show the relative error of the vertical stress versus different values of aspect ratio for patterns one and two. The magnitude of relative error is almost similar for pattern one (Fig. 11a) and the same data for the model 1 (Fig. 9a). Comparison of patterns one and two shows that the relative error is more sensitive to the mesh density (NTV) in pattern 2 (Fig. 11b). In other words, when the load is applied in the direction of the shortest edge of the element, a finer mesh size is needed to reach an acceptable error (5%).

Sensitivity analysis to different OR and element shape is presented in Figures 12a, b. The results (absolute error value) are similar to the model 1.

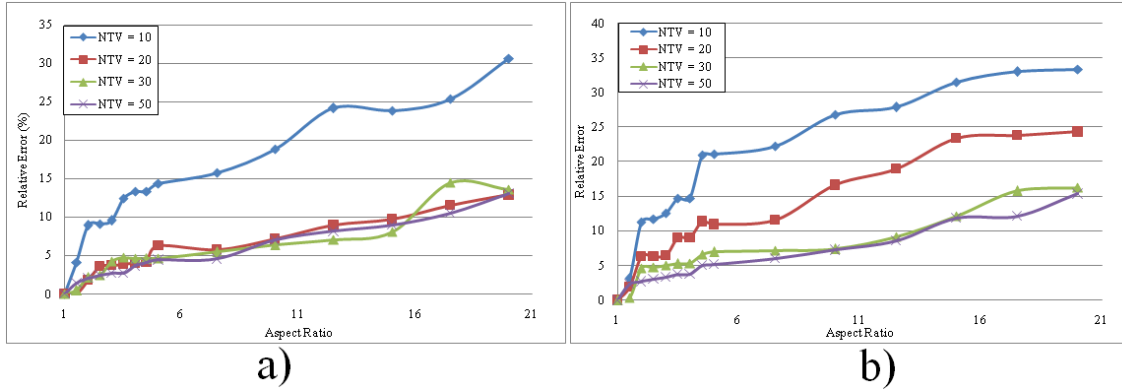


Figure 11. a) Aspect ratio sensitivity analysis (pattern one) for rough strip footing in an infinite Mohr-Coulomb material, b) Aspect ratio sensitivity analysis (pattern two) for rough strip footing in an infinite Mohr-Coulomb material.

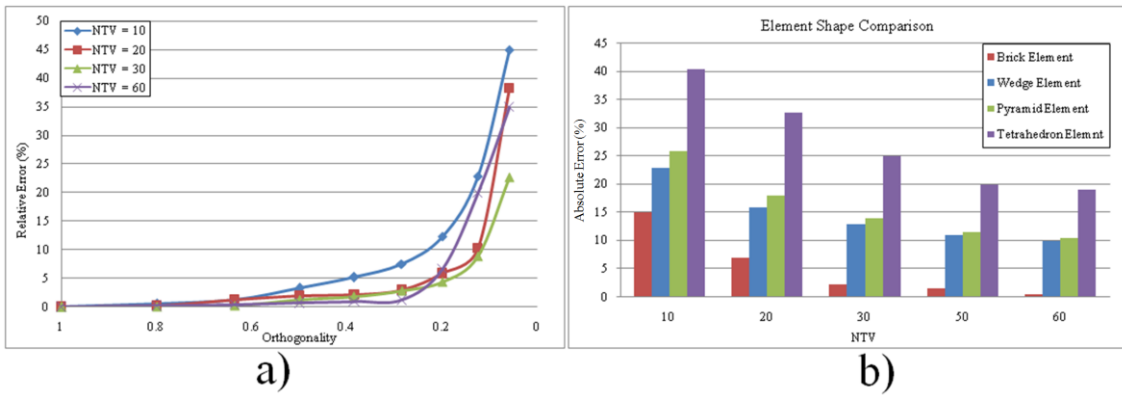


Figure 12. a) Orthogonality sensitivity analysis (pattern one) for rough strip footing in an infinite Mohr-Coulomb material, b) Zone shape sensitivity analysis (pattern one) for rough strip footing in an infinite Mohr-Coulomb material.

5.3 Smooth square footing on a cohesive frictionless material (model 3)

This problem simulates the 3-dimensional effect of aspect ratio, orthogonality and element shape in typical smooth square footing problem. Fifteen aspect ratios ($AR = 1$ to 20), nine orthogonality ratios ($OR = 1$ to 0.058) and four element shapes (brick, wedge, pyramid and tetrahedron) with different mesh densities ($NTV = 5$ to 63) were selected. The velocity contour,

plastic and load-displacement curve corresponding to the numerical and analytical simulation for $AR = 1$ and $NTV = 50$ is presented in Figure 13, in which p -load is the normalized average footing pressure (p/c), p -sol is the normalized upper bound value for the bearing capacity (q_u/c) and c -disp is the normalized vertical displacement (u_z/a) at the center of the footing. The numerical value of the bearing capacity is 541 kPa. This value is sandwiched between the theoretical upper-bound value of 571 kPa and lower-bound value of 514 kPa (Equation 2).

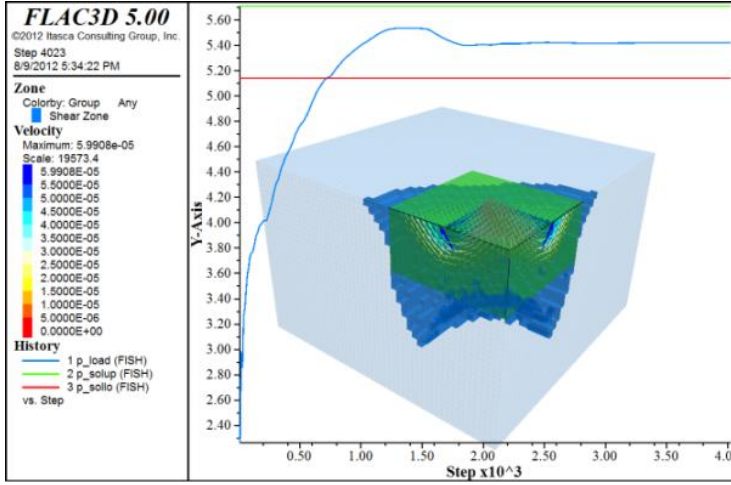


Figure 13. Stress and plastic zone comparison between analytical and $FLAC^{3D}$ solution.

Figure 14a shows the relative error of the vertical stress versus different value of aspect ratios for the NTV values of 10, 20, 30 and 50. For comparison it is assumed that a mesh element with $AR = 1$ (equal size element) is an ideal mesh with relative error of zero. The results show that relative errors remains below 5% when AR increases from 1.0 to 3.0. By increasing the mesh density to an NTV of 50 the relative error decreases significantly. In the case of a coarse to a relatively fine mesh size ($NTV = 10$ to 30) the relative error is between 5% and 10% for $AR = 2.5$ to 8.0. For an extremely fine mesh ($NTV = 50$) relative errors remain below 10% up to an AR of 15.0.

Figure 14b shows the relative error (the numerical analysis results are compared with the close form solution results) of the vertical stress versus different orthogonality ratios (OR) for the NTV values of 10, 20, 30 and 50. For this comparison it is assumed that a mesh element with $OR = 1.0$ (corresponding to right angle) is an ideal element with relative error of zero. The results show that relative error is sensitive to mesh density; for the coarse mesh ($NTV = 10$) this value remains below 5% as OR varies from 1.0 to 0.65 (corresponding to an acute angle of 58.5 degree) and for the fine mesh ($NTV = 20$ -50) as OR varies from 1.0 to 0.25 (corresponding to an acute angle of 22.5 degree). However, for OR values less than 0.25 (or acute angles of less than 22.5 degree) the relative error increases significantly.

Figure 14c shows the absolute error of the vertical stress versus different mesh element shapes for NTV values of 10, 20, 30, 50 and 60. The analyses show that the accuracy of results is extremely sensitive to mesh density. In coarse meshes ($NTV = 10$) brick element shapes yield a 20% error while tetrahedral elements yield an error of 65%. The brick element shape has the lowest absolute error and tetrahedral has the largest error. Between wedge and pyramid mesh shape wedge elements shows a slightly better performance. Tetrahedral mesh elements perform poorly even with an extremely fine mesh size (an error of 17% for $NTV = 60$).

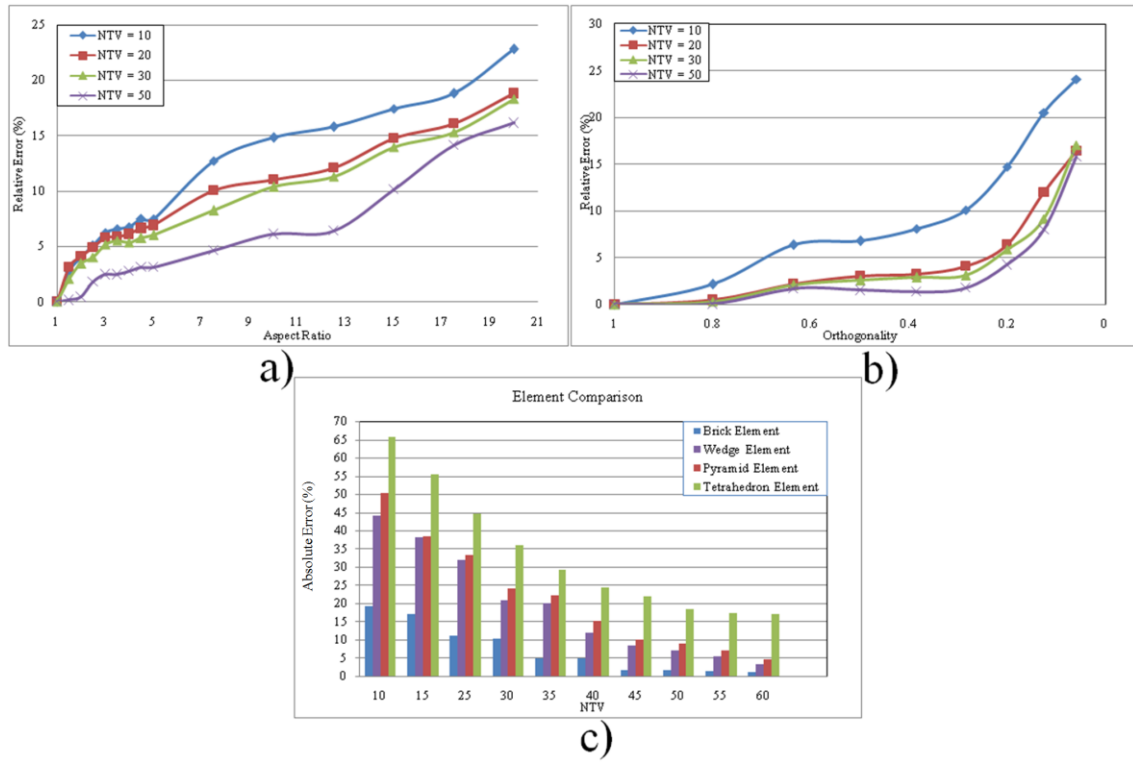


Figure 14. a) Aspect ratio sensitivity analysis (pattern one) for rough strip footing in an infinite Mohr-Coulomb material, b) Orthogonality sensitivity analysis (pattern one) for rough strip footing in an infinite Mohr-Coulomb material, c) Zone shape sensitivity analysis (pattern one) for rough strip footing in an infinite Mohr-Coulomb material.

6 SUMMARY AND CONCLUSION

Several tests were performed to analyze mesh quality in *FLAC^{3D}* software. The effect of different aspect ratio (AR), orthogonality ratio (OR) and mesh element shapes on the final solution and an estimate of the error that the user may expect were reported (Table 4).

Table 4. Relative error for different range of AR and OR.

Relative Error	Mesh density	Aspect Ratio (AR)		Orthogonality (OR)	
		2-D	3-D	2-D	3-D
< 5 %	NTV = 20	(1.0-5.0)	(1.0-3.0)	(1.00-0.28)	(1.00-0.28)
	NTV = 50	(1.0-7.5)	(1.0-8.0)	(1.00-0.26)	(1.00-0.18)
5- 10%	NTV = 20	(5.0-15.0)	(3.0-7.5)	(0.26-0.12)	(0.26-0.15)
	NTV = 50	(7.5-17.0)	(8.0-15.0)	(0.28-0.17)	(0.18-0.10)
10-15%	NTV = 20	(15.0-17.5)	(7.5-15.4)	(0.12-0.08)	(0.15-0.08)
	NTV = 50	(17.0-20.0)	(15.0-18.2)	(0.17-0.15)	(0.10-0.07)
15% <	NTV = 20	< 17.5	< 15.4	0.08 >	0.08 >
	NTV = 50	< 20.0	< 18.2	0.15 > 0	0.07 >

The following comments summarize the results shown in Table 4:

- Relative error remains low (less than 5%) for aspect ratio of (1.0 to 7.5) and (1.0 to 3.0) for 2-dimensional and 3-dimensional problem, respectively. This value is between 5% to 10% for aspect ratio of (7.5 to 15) and (3.0 to 10) for 2-dimensional and 3-dimensional problem, respectively. Using an aspect ratio outside this range requires a very dense mesh pattern.

- Relative error remains low (less than 5%) for orthogonality ratio of (1.0 to 0.38) and (1.0 to 0.65) for 2-dimensional and 3-dimensional problem, respectively. Using an orthogonality ratio outside this range increases the relative error significantly. Mesh density (NTV) does not improve the problem resolution significantly.
- Brick element mesh shape has the lowest absolute error and tetrahedral has the highest. Between the wedge and pyramid mesh shape wedge elements show slightly better performance. Tetrahedral mesh elements perform poorly even with the extremely fine mesh size.

REFERENCES

- Amenta, M. B. N. & Eppstein, D. 1997. Optimal point placement for mesh smoothing. *In: Proc. of the 8th ACM-SIAM Symposium on Discrete Algorithms*: 528–537.
- Chalasan, S., Thompson, D. & Soni, B. 2002. Topological adaptivity for mesh quality improvement. *Numerical Grid Generation in Computational Field Simulations*: 107–116.
- Chen, W.F. 1975. Bearing Capacity of Square, Rectangular and Circular Footings. *In Limit Analysis and Soil Plasticity, Developments in Geotechnical Engineering 7, Ch. 7*: 295–340. New York: Elsevier Scientific Publishing Co.
- Freitag, L. & Plassmann, P. 2000. Local optimization-based simplicial mesh untangling and improvement. *Int. J. Numer. Math. Eng. vol 49*: 109–125.
- Freitag, L. & Ollivier, C. 1997. Tetrahedral mesh improvement using swapping and smoothing. *Int. J. Num. Meth. Eng. Vol. 40*: 3979–4002.
- Itasca Consulting Group, Inc. 2012. *FLAC^{3D} — Fast Lagrangian Analysis of Continua in Three-Dimensions, Ver. 5.0*. Minneapolis: Itasca.
- Joe, B. 1995. Construction of three-dimensional improved-quality triangulations using local transformations. *SIAM J. Sci. Comp. vol. 16*: 1292–1307.
- Klein, R. 1999. Star formation with 3-D adaptive mesh refinement: the collapse and fragmentation of molecular clouds. *J. Comput. Appl. Math vol 109*: 123–152.
- Knupp, P. 2003. Algebraic Mesh Quality Measures for Unstructured Initial Meshes. *Finite Elements in Design and Analysis*: 217–241
- Knupp, P. 2007. Remarks on Mesh Quality. *45th AIAA Sciences Meeting and Exhibit*: 0933. Reno, NV.
- Knupp, P. 2009. Label-Invariant Mesh Quality Metrics. *Proceedings of the 18th International Meshing Roundtable*: 139–155. Springer, Heidelberg.
- Kwok, W. & Chen, Z. 2000. A simple and elective mesh quality metric for hexahedral and wedge elements. *In: Proceedings of the 9th International Meshing Roundtable*: 325–333. New Orleans LA.
- Pebay, P. 2004. Planar quadrangle quality measures. *Engr. w/Comp. 20(2)*: 157–173.
- Robinson, J. 1987. CRE method of element testing and the Jacobian shape parameters. *Eng. Comput. 4*: 113–118.
- Salençon, J. 1969. Contraction Quasi-Statique D’une Cavité à Symétrie Sphérique Ou Cylindrique Dans Un Milieu Elastoplastique. *Annales Des Ponts Et Chaussées vol. 4*: 231–236.
- Shield, R.T. & Drucker, D.C. 1953. The Application of Limit Analysis to Punch-Indentation Problems. *J. Appl. Mech., vol. 20*: 453–460.
- Sloan, S.W. & Randolph, M.F. 1982. Numerical Prediction of Collapse Loads Using Finite Element Methods. *Int. J. Num. & Anal. Methods in Geomech., vol. 6*: 47–76.
- Stimpson, C., Ernst, C., Knupp, P., Pebay, P. & Thompson, D. 2007. The Verdict Geometric Quality Library. *SAND*: 1751. Sandia National Laboratories.
- Tamassia, R., Tollis, I. G. & Vitter, J. S. 1991. A Parallel Algorithm for Planar Orthogonal Grid Drawings. *SIAM Journal on Computing, 20(4)*: 708–725.
- Terzaghi, K. & Peck, R.B. 1967. *Soil Mechanics in Engineering Practice, 2nd Ed.* New York: John Wiley and Sons.